Band Alignments, Band Gap, Core-levels and Valence-Band States in Cu_3BiS_3 for Photovoltaics - Supplementary Information

Thomas J. Whittles,[†] Tim D. Veal,[†] Christopher N. Savory,[‡,∥] Peter J. Yates,[†] Philip A. E. Murgatroyd,[†] James T. Gibbon,[†] Max Birkett,[†] Richard J. Potter,[¶] Jonathan D. Major,[†] Ken Durose,[†] David O. Scanlon,[‡,§,∥] and Vinod R. Dhanak[*,†]

[†]*Department of Physics and Stephenson Institute for Renewable Energy, University of Liverpool, Liverpool, L69 7ZF, United Kingdom*

[‡]*Department of Chemistry, University College London, Christopher Ingold Building, London WC1H 0AJ, United Kingdom*

[¶]*Department of Mechanical, Materials and Aerospace Engineering, School of Engineering, University of Liverpool, Liverpool, L69 3GH, United Kingdom*

[§]*Diamond Light Source Ltd., Diamond House, Harwell Science and Innovation Campus, Didcot, Oxfordshire OX11 0DE, United Kingdom*

[∥]*Thomas Young Centre, University College London, Gower Street, London WC1E 6BT, United Kingdom*

E-mail: Vin@liverpool.ac.uk

1 XPS Survey Spectra

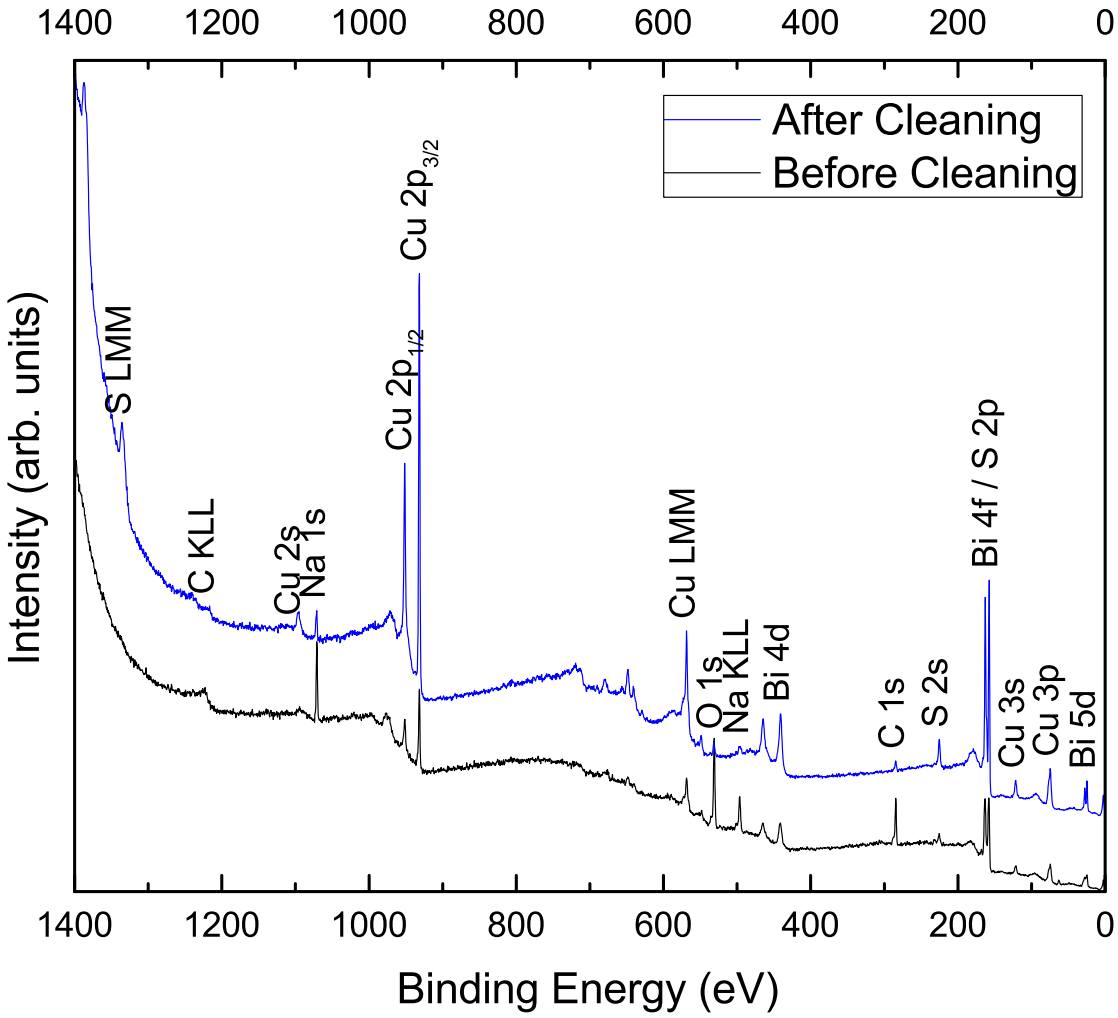

Figure S1: XPS survey spectra for the CBS sample before and after surface cleaning.

The survey spectra for CBS before and after surface cleaning are shown in Figure S1 and are discussed in section 3.2 of the main text. Further discussion of the possible effects of sodium and the other contaminants can be found in section 4 below, along with the associated XPS spectra.

2 XPS Core Level Fitting Procedure for Bi and S

The difference in spin-orbit splitting of the Bi $4f$ and S $2p$ doublets should help with confidently fitting the spectra. However this is complicated by the fact that even though, stoichiometrically speaking, the sulphur signal should be three times greater than the bismuth signal, it will in fact be much (5.5 times) weaker than the bismuth signal when taking the differences in photoionisation cross sections into account.[1] This problem is further compounded by the likelihood of oxidation present on the surface of the material, which would cause further peak overlap within the region. The possibility of oxidation also prevents the centroid value of the peak from being representative of the material, because it would cause the centroid binding energy to skew.

Because of the multi-component complexity of the overlapping region of the Bi $4f$ and S $2p$ doublets, the S $2s$ and Bi $4d$ regions were also recorded in order to corroborate the fitting. These two regions should be representative of the main doublets, because as they lie within a similar kinetic energy range for the ejected photoelectrons, their inelastic mean free paths are similar,[2] the photoelectron escape depths are similar and therefore the ratios between the area of a bulk (CBS) and surface species (Bi_2O_3/S-O) should be the same. Also, in order to create a robust fit that can be propagated to other samples, some assumptions must be made in order to prevent an unmanageable number of variables. Firstly, it was assumed that any peaks that did not arise from CBS will not shift BE due to cleaning or annealing, will only change in intensity and/or FWHM,[3] and therefore were fixed to the BE that was measured in the sample before surface cleaning. The spectra before surface cleaning was used because here the contaminant peaks are largest and therefore this is where one has most confidence in the fitted BE. Secondly, the number of species of an element is the same no matter which orbital is being used and the ratios between the species within an orbital will be the same when considering different orbitals. This will be true for the areas of the peaks, because although the photoionisation cross sections will be different between orbitals, they are the same within an orbital. This will also be true for the FWHM of the peaks, because although

the core-hole lifetimes will be different for the different species and different orbitals, it will be the same difference between the orbitals as the instrumental broadening remains the same throughout. Hence, for the other corroborative regions, these ratios were fixed. Finally, it is estimated that the Bi $5s$ peak should lie within this overlap region as well,[4] however because there are no reports on this peak with regards to fitting or BE shifts, it shall not be included in the model used here as most likely it will be very small. Nevertheless it is recognised that some intensity may arise because of it. Bearing these assumptions in mind, the fitting procedure used for the Bi and S peaks for CBS can be summarised as follows:

1. Determine the number, FWHM ratio and area ratio of S peaks for the sample before cleaning using the S $2s$ region.

2. Translate these peaks into S $2p$ doublets using appropriate constraints.

3. Determine the number, FWHM ratio and area ratio of Bi peaks for the sample before cleaning by modelling the remaining intensity in the overlap region with Bi $4f$ doublets.

4. Translate these doublets into Bi $4d$ doublets using appropriate constraints.

5. Translate all the above steps to the sample after cleaning to determine the effect of cleaning in terms of peak intensity and BE shifts for the peaks associated with CBS.

The sample before surface cleaning was chosen to be fitted first as these spectra contain the greater number of prominent peak crests, giving better confidence to the number of peaks chosen. The S $2s$ region was fitted first, as this would give the number of small S $2p$ peaks present in the overlap region, allowing more confidence in the number and position of the larger Bi $4f$ peaks. Three peaks were determined in this region for the sample before cleaning, as shown in the bottom spectra in Figure S2. This then reduced to two peaks after cleaning, where one of the peaks is almost insignificant. The assignment for these peaks are in agreement with those for S $2p$ that are described in the main text. The peak at higher BE which is removed after cleaning (pink dot) is attributed to sulphur bonded to oxygen with

+6 valency because of the large shift from sulphide to sulphate species.[5] The peak around 228 eV is S-C (green dash dot), which decreases after cleaning and is in agreement with the corresponding S 2p doublet and literature values,[6] and the strongest peak (red dash) is due to S with -2 valency in CBS, which is in agreement with the corresponding S 2p doublet.

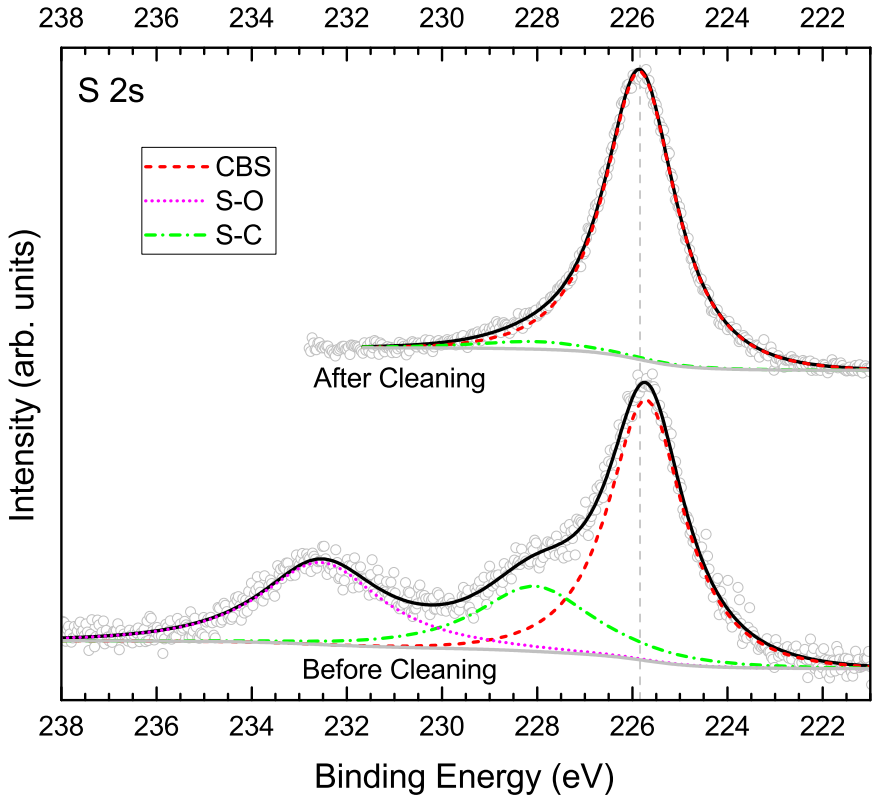

Figure S2: XPS spectra for the S 2s region of the CBS sample before and after surface cleaning. Peak envelope shown in black.

The S 2s peaks are then converted to S 2p doublets, using the appropriate constraints, as detailed in the main text, and are fixed with regards to area and FWHM ratios. The remaining area in the overlap region is then taken up by Bi 4f doublets. An initial model used two doublets for the sample before cleaning, one for Bi in CBS (red dash) and another at higher BE for oxidised bismuth (pink dot), these two doublets are evident from the peak crests seen in Figure S3. Attempting to optimise the fit described above (three S 2p doublets and two Bi 4f doublets) for the Bi 4f/S 2p region of the sample before cleaning resulted in an unsatisfactory fit for several reasons which are illustrated in the top spectra of Figure S3.

There is always missing intensity at low BE around 157 eV (α), the S 2p doublet attributed to S-C (green shading) fits with a BE (β) that is too close to the BE of the S 2p doublet associated with CBS (red shading) to be in agreement with the literature,[7] and several other features (γ) where the model either under- or overcompensates the experimental data. This suggests that another Bi doublet is present because of the missing intensity around 157 and 163 eV, which also corresponds to the doublet separation for Bi 4f. A doublet around this BE would be consistent with metallic bismuth (also shown in Figure S3 is a metallic bismuth spectrum from an independently measured Bi foil), and reasons for this assignment are discussed in the main text. Confidence in this extra species is heightened by the fact that without it, line shape and background alterations would not give a better fit. With this doublet included (blue dash dot), a much more robust fit is achieved, as shown in the middle spectra of Figure S3, and it is this model which is propagated to the clean sample, which also gives a satisfactory fit. The area of the metallic bismuth peaks are relatively small, and as such do not affect the BE of the other peaks. It is noted that the line shape of metallic species should be asymmetric,[8] however because of the relative intensity of this species and the added complexity associated with asymmetrical line shapes, a symmetrical line shape models this species satisfactorily. The assignments for the peaks in this region can be found in the main text.

The Bi 4d region was fitted only as corroboration to the peak model adopted in the overlap region and not as a dictatorial region like the S 2s region. This is because there are many reports on the S 2s region being used as an alternative[9–21] but few on using the Bi 4d region,[11] hence, there is less confidence in the fitting used here. Also, the Bi 4d region has a poorer SNR because the intensity is lower and also, as evidenced in Figure S4, the width for these peaks is very large, meaning that peaks will greatly overlap and as such, there will be less confidence using this region for an initial fit. Nevertheless, a corroborative fit was achieved which is in agreement with the model used for the overlap region. The doublets were constrained to have 23.7 eV[4,22] separation and an area ratio of 2:3. Due to the size of

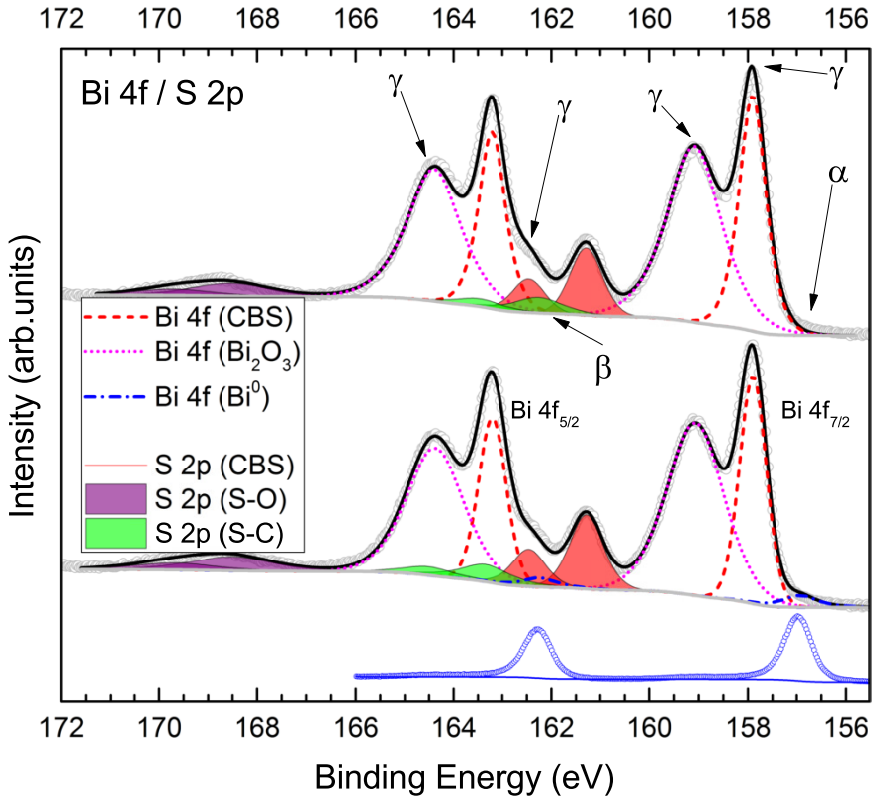

Figure S3: XPS spectra for the Bi $4f$ and S $2p$ overlap region of the CBS sample with (middle) and without (top) including a contribution from metallic bismuth. Peak envelope is shown in black. Shown at the bottom is a Bi $4f$ spectrum from a Bi foil.

the metallic bismuth peak (blue dash dot), the BE was constrained to the standard reference energy for metallic Bi $4d_{5/2}$ at 440 eV,[4] in agreement with the Bi $4f_{7/2}$ peak located at the standard value for metallic bismuth as well. Background subtraction proved difficult here because the region lies toward the lower BE side of the Cu LMM Auger features, creating a steeply rising background, as can be seen in Figure S4. As such, a Shirley background did not give a good fit, so a Tourgaard background was used.[23] It is believed that a modified Shirley background would provide the best fit, however this is unnecessary for this region. Using the appropriate constraints, reasonable fits were achieved for the sample both before and after cleaning, strengthening confidence in the fit within the overlapping region. The largest peak in this region (red dash) corresponds to Bi in CBS, as it is in the overlap region, and the peak at higher BE (pink dot) is due to Bi_2O_3, in agreement with the literature.[11]

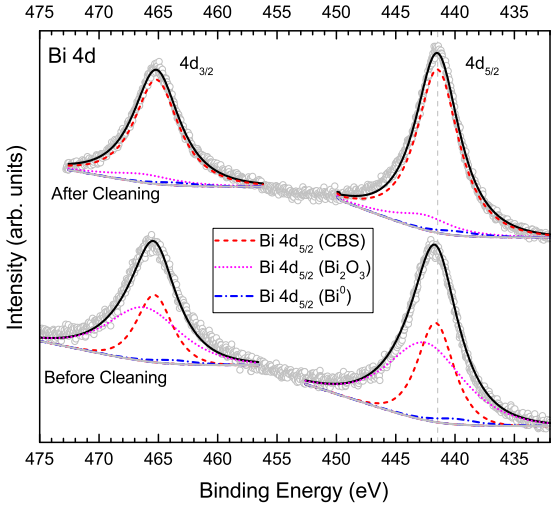

Figure S4: XPS spectra for the Bi $4d$ region of the CBS sample before and after surface cleaning. Peak envelope shown in black.

Binding energies for the peaks described above along with all other fitted peaks are shown in Table S1.

Table S1: XPS binding energies determined for all the peaks fitted to the CBS sample before and after surface cleaning. All values given in eV and the peak FWHM are given in parentheses.

	Cu_3BiS_3					Bi_2O_3		
Sample	Cu $2p_{3/2}$	Bi $4f_{7/2}$	S $2p_{3/2}$	Bi $4d_{5/2}$	S $2s$	Bi $4f_{7/2}$	Bi $4d_{5/2}$	O $1s$
Before cleaning	932.01 (1.16)	157.89 (0.65)	161.28 (0.81)	441.63 (3.54)	225.71 (1.87)	159.06 (1.37)	442.52 (7.47)	529.63 (0.99)
After cleaning	932.23 (1.05)	158.19 (0.77)	161.47 (0.78)	441.47 (4.22)	225.84 (1.75)	159.06 (1.02)	442.51 (5.61)	529.63 (1.00)

	Contamination							
Sample	Bi $4f_{7/2}$ (Bi^0)	Bi $4d_{5/2}$ (Bi^0)	O $1s$ (adv.)	S $2p_{3/2}$ (S-C)	S $2s$ (S-C)	S $2p_{3/2}$ (S-O)	S $2s$ (S-O)	Na $1s$
Before cleaning	156.94 (0.82)	440.00 (4.49)	531.74 (1.84)	163.33 (1.23)	228.04 (2.84)	168.50 (2.04)	232.55 (2.97)	1071.68 (1.54)
After cleaning	156.94 (0.82)	440.00 (4.51)	531.94 (2.19)	163.33 (1.26)	228.04 (2.84)	–	–	1071.93 (1.60)

3 Comparison with previous literature on XPS of CBS

Only two studies of CBS presented XPS spectra of the overlap region where a fitting model was used. However, one[24] reported binding energies which do not agree with the values measured here, possibly because of poor fitting of the spectrum, evidenced by the missing intensity, and although the other[25] reports a BE for Bi $4f_{7/2}$ which is in agreement with the value measured here, they both model the S $2p$ doublet as a very wide, single peak, suggesting there may be other species present which are unaccounted for. Taking inspiration from some studies of Bi_2S_3,[10–21] which experiences the same problem, one study of CBS recognised the problems associated with this overlapping region, and as such, chose to measure and report the S $2s$ region as well.[9] However, to ignore the S $2p$ contribution detracts from the problem that one or several underlying peaks can skew the Bi $4f$ peak positions from the centroid values. This, coupled with the poor quality data presented in that study, is believed to be partly responsible for the disagreement between the previously reported values and the ones shown in Table 1. Some studies of CBS,[9,26,27] report Bi $4f_{7/2}$ binding energies that are in agreement with the values measured in this study, and due to the size of the Bi $4f$ peaks compared to the S $2p$, these are taken to be representative of the material. Other studies of CBS present high quality XPS data, but these unfortunately suffer from a lack of fitting of the multi-component regions[28] or the presence of contaminants such as Bi_2O_3, but reporting no binding energies and as such, giving no corroboration to previous literature. A similar situation exists elsewhere with the presence of other species being explicitly excluded in the discussion without corroborative fitting evidence.[9,29] Still other studies are limited by not presenting or reporting the BEs for a full set of spectra,[28–30] and finally, some present and report S $2p$ spectra which are completely independent of the Bi $4f$ features,[9,26,27] suggesting fitting and subtraction of the Bi $4f$ peaks has been performed. However, with no discussion or explanation, this method is questionable. Given these weaknesses in the literature for CBS, it is believed that the spectra presented here, having taken all features into account, can provide a foundation onto which further studies of CBS can be supported in order to

progress further development. Also, because of the similar Bi-S crystal structure units for CBS and Bi_2S_3,[31,32] it is expected that Bi $4f_{7/2}$ and S $2p_{3/2}$ BEs should be comparable for both materials and the values measured here are in general agreement with representative studies of Bi_2S_3 in the literature.[10,11,15,27,33,34]

4 Contamination

The C 1*s*, O 1*s* and Na 1*s* regions for the CBS sample before and after cleaning were also recorded and are presented in Figure S5, with the binding energies found in Table S1.

The C 1*s* spectra for the sample before cleaning shows three peaks (orange dash) which are all attributed to the different bonding regimes associated with adventitious hydrocarbon contamination.[35] These reduce to two peaks after cleaning. The prominent peak was used for the charge correction as described in the main text and is generally associated with C-H or C-C bonds.[35]

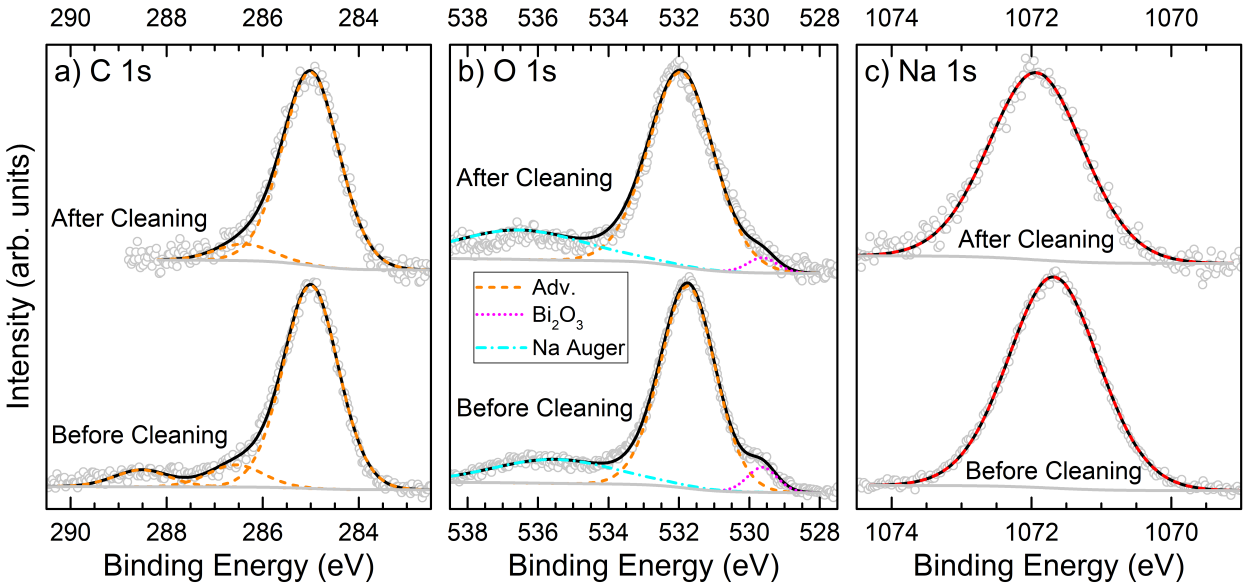

Figure S5: XPS spectra for the contamination regions of the CBS sample before and after surface cleaning. a) C 1*s* region, b) O 1*s* and Na Auger region, c) Na 1*s* region. Peak envelope shown in black.

The O 1*s* spectra both before and after surface cleaning show three features. The wide,

low intensity feature at high BE (cyan dash dot) is due to the Auger features of sodium. This complicates the fitting of this region because the spectral shape of this feature is unknown and therefore we have less confidence in the further fitting of the O 1s peaks. Nevertheless, there are two definite O 1s peaks present both before and after cleaning. The main peak with highest intensity (orange dash) is attributed to adventitious oxygen[36] and the small peak at lower BE (pink dot) is the oxygen from oxidised bismuth, which is in agreement with the literature[37,38] and is further discussed in the main text. Both O 1s peaks reduce on cleaning, suggesting that they are both present at the surface of the sample. Although one peak has been used for the adventitious oxygen, it is believed that in the sample before surface cleaning, the peak from the sulphur bonded to oxygen (evidenced from the S 2p spectrum) also resides around this energy.[39] This was not fitted further due to the complications associated with the sodium Auger features.

The Na 1s region was fitted with one peak both before and after cleaning (red dash), however it is noted that any shifts in the Na 1s peak are very small so it is possible that more than one species is present. The shift seen in this peak before and after the surface cleaning is consistent with the shift of the VBM suggesting that the sodium is incorporated with the material, because peaks associated with CBS also shift by this amount before and after cleaning. The impact of the presence of sodium is discussed in the main text.

5 Stoichiometry

The XPS spectra shown here have been normalised in order to more clearly show the different species present. Therefore, the atomic percentages derived from XPS are shown in Table S2. The values shown here correspond to the amount of material probed by the XPS technique and are therefore dependent both on element, and also the BE of the associated orbital, because different inelastic mean free paths and photoionisation cross sections will apply and no transmission function correction was available for the instrumentation used here. Absolute

values are therefore not exact and should be interpreted with caution, however comparisons between values and also trends before and after cleaning are more appropriate. In order to compare the stoichiometry values of the CBS material, absolute corrections were applied to the Cu/S ratios which derived from independent stoichiometry measurements of CuS and Cu_2S powders.[40] Relative sensitivity factor corrections[41] were applied to the Bi/S ratios as the transmission function should not have much effect between the Bi $4f$ and S $2p$ regions as they are energetically similar.

Table S2: Atomic percentages derived from XPS measurements for CBS before and after surface cleaning.

	Cu_3Bi_3			Bi_2O_3		Contamination					
	Cu	Bi	S	Bi	O	Bi^0	O (adv.)	S (S-C)	S (S-O)	Na	C (adv.)
Before cleaning	3.9	1.5	7.3	2.4	1.9	0.1	27.7	2.8	3.7	20.9	27.8
After cleaning	23.4	10.1	29.8	1.2	0.4	0.3	11.0	1.3	0.0	9.7	12.7

Therefore, in Cu_3BiS_3 the expected ratio of Cu:Bi:S should be 3:1:3. By normalising to a Bi content of 1, the stoichiometry of the CBS sample before cleaning is 2.6:1.0:4.9 and after cleaning is 2.3:1.0:2.9. Further discussion of these values and their implications can be found in the main text.

Also, as can be seen, after cleaning, all of the contaminants reduce compared with the CBS. In fact, the ratio of bismuth in CBS to bismuth which makes up the oxide layer reduces from 1.0:1.6 before cleaning to 1.0:0.1 after cleaning.

References

(1) Yeh, J. J.; Lindau, I. Atomic Subshell Photoionization Cross Sections and Asymmetry Parameters: $1 \leq Z \leq 103$. *At. Data Nucl. Data Tables* **1985**, *32*, 1–155.

(2) Powell, C. J.; Jablonski, A.; Salvat, F. NIST Databases with Electron Elastic-Scattering Cross Sections, Inelastic Mean Free Paths, and Effective Attenuation Lengths. *Surf. Interface Anal.* **2005**, *37*, 1068–1071.

(3) Nelin, C. J.; Bagus, P. S.; Brown, M. A.; Sterrer, M.; Freund, H. J. Analysis of the Broadening of X-Ray Photoelectron Spectroscopy Peaks for Ionic Crystals. *Angew. Chemie - Int. Ed.* **2011**, *50*, 10174–10177.

(4) Nyholm, R.; Berndtsson, A.; Mårtensson, N. Core Level Binding Energies for the Elements Hf to Bi (Z=72–83). *J. Phys. C Solid State Phys.* **1980**, *13*, L1091–L1096.

(5) Zingg, D. S.; Hercules, D. M. Electron Spectroscopy for Chemical Analysis Studies of Lead Sulfide Oxidation. *J. Phys. Chem.* **1978**, *82*, 1992–1995.

(6) Vargo, T. G.; Gardella Jr., J. A. Development of Ti K_α X Radiation for Electron Spectroscopy for Chemical Analysis of Polymer Surfaces. *J. Vac. Sci. Technol. A* **1989**, *7*, 1733.

(7) Paraknowitsch, J. P.; Thomas, A.; Schmidt, J. Microporous Sulfur-Doped Carbon from Thienyl-Based Polymer Network Precursors. *Chem. Commun.* **2011**, *47*, 8283–8285.

(8) Doniach, S.; Sunjic, M. Many-Electron Singularity in X-Ray Photoemission and X-Ray Line Spectra from Metals. *J. Phys. C Solid State Phys.* **1970**, *3*, 285–291.

(9) Yin, J.; Jia, J. Synthesis of Cu_3BiS_3 Nanosheet Films on TiO_2 Nanorod Arrays by a Solvothermal Route and Their Photoelectrochemical Characteristics. *CrystEngComm* **2014**, *16*, 2795.

(10) Grigas, J.; Talik, E.; Lazauskas, V. X-Ray Photoelectron Spectra and Electronic Structure of Bi_2S_3 Crystals. *Phys. Stat. Sol. (b)* **202**, *232*, 220–230.

(11) Debies, T. P.; Rabalais, J. W. X-Ray Photoelectron Spectra and Electronic Structure of Bi2X3 (X = O, S, Se, Te). *Chem. Phys.* **1977**, *20*, 277–283.

(12) Chen, R.; So, M. H.; Che, C.-M.; Sun, H. Controlled Synthesis of High Crystalline Bismuth Sulfide Nanorods: Using Bismuth Citrate as a Precursor. *J. Mater. Chem.* **2005**, *15*, 4540–4545.

(13) Fang, Z.; Liu, Y.; Fan, Y.; Ni, Y.; Wei, X.; Tang, K.; Shen, J.; Chen, Y. Epitaxial Growth of CdS Nanoparticle on Bi_2S_3 Nanowire and Photocatalytic Application of the Heterostructure. *J. Phys. Chem. C* **2011**, *115*, 13968–13976.

(14) Liao, X.-H.; Wang, H.; Zhu, J.-J.; Chen, H.-Y. Preparation of Bi2S3 Nanorods by Microwave Irradiation. *Mater. Res. Bull.* **2001**, *36*, 2339–2346.

(15) Liufu, S.-C.; Chen, L.-D.; Yao, Q.; Wang, C.-F. Bismuth Sulfide Thin Films with Low Resistivity on Self-Assembled Monolayers. *J. Phys. Chem. B* **2006**, *110*, 24054–24061.

(16) Panigrahi, P. K.; Pathak, A. The Growth of Bismuth Sulfide Nanorods from Spherical-Shaped Amorphous Precursor Particles under Hydrothermal Condition. *J. Nanoparticles* **2013**, *2013*, 367812:1–11.

(17) Purkayastha, A.; Yan, Q.; Raghuveer, M. S.; Gandhi, D. D.; Li, H.; Liu, Z. W.; Ramanujan, R. V.; Borca-Tasciuc, T.; Ramanath, G. Surfactant-Directed Synthesis of Branched Bismuth Telluride/Sulfide Core/Shell Nanorods. *Adv. Mater.* **2008**, *20*, 2679–2683.

(18) Tamašauskaitė Tamašinaitė, L.; Šimknaitė Stanynienė, B.; Naruškevičius, L.; Valiulienė, G.; Žielienė, A., A.; Sudavičius EQCM Study of Electrochemical Modification of Bi_2S_3 Films in the Zn^{2+}-Containing Electrolyte. *J. Electroanal. Chem.* **2009**, *633*, 347–353.

(19) Tamašauskaitė-Tamašinaitė, L.; Valiulienė, G.; Žielienė, A.; Šimknait Stanynienė, B.; Naruškevičius, L.; Sudavičius, A. EQCM Study on the Oxidation/reduction of Bismuth Sulfide Thin Films. *J. Electroanal. Chem.* **2010**, *642*, 22–29.

(20) Wang, H.; Zhu, J.-J.; Zhu, J.-M.; Chen, H.-Y. Sonochemical Method for the Preparation of Bismuth Sulfide Nanorods. *J. Phys. Chem. B* **2002**, *106*, 3848–3854.

(21) Zhong, J.; Xiang, W.; Liu, L.; Yang, X.; Cai, W.; Zhang, J.; Liang, X. Biomolecule-Assisted Solvothermal Synthesis of Bismuth Sulfide. *Nanorods. J. Mater. Sci. Technol.* **2010**, *26*, 417–422.

(22) Shalvoy, R. B.; Fisher, G. B.; Stiles, P. J. Bond Ionicity and Structural Stability of Some Average-Valence-Five Materials Studied by X-Ray Photoemission. *Phys. Rev. B* **1977**, *15*, 1680–1697.

(23) Repoux, M. Comparison of Background Removal Methods for XPS. *Surf. Interface Anal.* **1992**, *18*, 567–570.

(24) Murali, B.; Madhuri, M.; Krupanidhi, S. B. Near-Infrared Photoactive Cu_3BiS_3 Thin Films by Co-Evaporation. *J. Appl. Phys.* **2014**, *115*, 173109.

(25) Yan, J.; Yu, J.; Zhang, W.; Li, Y.; Yang, X.; Li, A.; Yang, X.; Wang, W.; Wang, J. Synthesis of Cu_3BiS_3 and $AgBiS_2$ Crystallites with Controlled Morphology Using Hypocre-

llin Template and Their Catalytic Role in the Polymerization of Alkylsilane. *J. Mater. Sci.* **2012**, *47*, 4159–4166.

(26) Hu, J.; Deng, B.; Wang, C.; Tang, K.; Qian, Y. Convenient Hydrothermal Decomposition Process for Preparation of Nanocrystalline Mineral Cu_3BiS_3 and $Pb_{1-x}Bi_{2x/3S}$. *Mater. Chem. Phys.* **2003**, *78*, 650–654.

(27) Zhong, J.; Xiang, W.; Cai, Q.; Liang, X. Synthesis, Characterization and Optical Properties of Flower-like Cu_3BiS_3 Nanorods. *Mater. Lett.* **2012**, *70*, 63–66.

(28) Nair, P. K.; Huang, L.; Nair, M. T. S.; Hu, H.; Meyers, E. A.; Zingaro, R. A. Formation of p-Type Cu_3BiS_3 Absorber Thin Films by Annealing Chemically Deposited Bi_2S_3-CuS Thin Films. *J. Mater. Res.* **1997**, *12*, 651–656.

(29) Mesa, F.; Chamorro, W.; Vallejo, W.; Baier, R.; Dittrich, T.; Grimm, A.; Lux-Steiner, M. C.; Sadewasser, S. Junction Formation of Cu_3BiS_3 Investigated by Kelvin Probe Force Microscopy and Surface Photovoltage Measurements. *Beilstein J. Nanotechnol.* **2012**, *3*, 277–284.

(30) Mesa, F.; Dussan, A.; Gordillo, G. Study of the Growth Process and Optoelectrical Properties of Nanocrystalline Cu_3BiS_3 Thin Films. *Phys. Stat. Sol. (c)* **2010**, *7*, 917–920.

(31) Lundegaard, L. F.; Makovicky, E.; Boffa-Ballaran, T.; Balic-Zunic, T. Crystal Structure and Cation Lone Electron Pair Activity of Bi_2S_3 between 0 and 10 GPa. *Phys. Chem. Miner.* **2005**, *32*, 578–584.

(32) Caracas, R.; Gonze, X. First-Principles Study of the Electronic Properties of A_2B_3 Minerals, with A=Bi,Sb and B=S,Se. *Phys. Chem. Miner.* **2005**, *32*, 295–300.

(33) Lou, W.; Chen, M.; Wang, X.; Liu, W. Novel Single-Source Precursors Approach to

Prepare Highly Uniform Bi_2S_3 and Sb_2S_3 Nanorods via a Solvothermal Treatment. *Chem. Mater.* **2007**, *19*, 872–878.

(34) Yang, X.; Wang, X.; Zhang, Z. Facile Solvothermal Synthesis of Single-Crystalline Bi_2S_3 Nanorods on a Large Scale. *Mater. Chem. Phys.* **2006**, *95*, 154–157.

(35) Barr, T. L.; Seal, S. Nature of the Use of Adventitious Carbon as a Binding Energy Standard. *J. Vac. Sci. Technol. A* **1995**, *13*, 1239.

(36) Payne, B. P.; Biesinger, M. C.; McIntyre, N. S. X-Ray Photoelectron Spectroscopy Studies of Reactions on Chromium Metal and Chromium Oxide Surfaces. *J. Electron Spect. Rel. Phenomena* **2011**, *184*, 29–37.

(37) Dharmadhikari, V. S.; Sainkar, S. R.; Badrinarayan, S.; Goswami, A. Characterisation of Thin Films of Bismuth Oxide by X-Ray Photoelectron Spectroscopy. *J. Electron Spectros. Relat. Phenomena* **1982**, *25*, 181–189.

(38) Uchida, K.; Ayame, A. Dynamic XPS Measurements on Bismuth Molybdate Surfaces. *Surf. Sci.* **1996**, *357–358*, 170–175.

(39) Lindberg, B. J.; Hamrin, K.; Johansson, G.; Gelius, U.; Fahlman, A.; Nordling, C.; Siegbahn, K. Molecular Spectroscopy by Means of ESCA II. Sulfur Compounds. Correlation of Electron Binding Energy with Structure. *Phys. Scr.* **1970**, *1*, 286–298.

(40) Whittles, T. J. *PhD Thesis: Electronic Characterisation of Earth-Abundant Sulphides for Solar Photovoltaics*; Springer, 2018.

(41) Wagner, C. D.; Davis, L. E.; Zeller, M. V.; Taylor, J. A.; Raymond, R. H.; Gale, L. H. Empirical Atomic Sensitivity Factors for Quantitative Analysis by Electron Spectroscopy for Chemical Analysis. *Surf. Interface Anal.* **1981**, *3*, 211–225.